frontiers in Astronomy and Space Sciences

ORIGINAL RESEARCH
published: 14 July 2021
doi: 10.3389/fspas.2021.667058

Quenching of Isovector and Isoscalar Spin-M1 Excitation Strengths in $N = Z$ Nuclei

Hiroaki Matsubara[1,2]* *and Atsushi Tamii*[1]

[1]Research Center for Nuclear Physics (RCNP), Osaka University, Ibaraki, Japan, [2]Department of Radiology, Kyoto Prefectural University of Medicine, Kyoto, Japan

Spin-$M1$ excitations of nuclei are important for describing neutrino reactions in supernovae or in neutrino detectors since they are allowed transitions mediated by neutral current neutrino interactions. The spin-$M1$ excitation strength distributions in self-conjugate $N = Z$ nuclei were studied by proton inelastic scattering at forward angles for each of isovector and isoscalar excitations as reported in H. Matsubara et al., Phys. Rev. Lett. **115**, 102501 (2015). The experiment was carried out at the Research Center for Nuclear Physics, Osaka University, employing a proton beam at 295 MeV and the high-resolution spectrometer Grand Raiden. The measured cross-section of each excited state was converted to the squared nuclear matrix elements of spin-$M1$ transitions by applying a unit cross-section method. Comparison with predictions by a shell-model has revealed that isoscalar spin-$M1$ strengths are not quenched from the prediction although isovector spin-$M1$ strengths are quenched similarly with Gamow-Teller strengths in charged-current reactions. This finding hints at an important origin of the quenching of the strength relevant to neutrino scattering, that is, the proton-neutron spin-spin correlation in the ground state of the target nucleus. In this manuscript we present the details of the unit cross-section method used in the data analysis and discuss the consistency between the quenching of the isoscalar magnetic moments and that of the isoscalar spin-M1 strengths.

Keywords: Sd-shell nuclei, shell-model calculation, proton inelastic scattering, spin-M1 transition, GT-transition

OPEN ACCESS

Edited by:
Francesco Cappuzzello, University of Catania, Italy

Reviewed by:
Marco Martini, Institut Polytechnique des Sciences Avancées, France
Zhenbin Wu, University of Illinois at Chicago, United States

***Correspondence:**
Hiroaki Matsubara
mats.hiroaki@gmail.com

Specialty section:
This article was submitted to High-Energy and Astroparticle Physics, a section of the journal Frontiers in Astronomy and Space Sciences

Received: *11 February 2021*
Accepted: *14 June 2021*
Published: *14 July 2021*

Citation:
Matsubara H and Tamii A (2021) Quenching of Isovector and Isoscalar Spin-M1 Excitation Strengths in N = Z Nuclei. Front. Astron. Space Sci. 8:667058. doi: 10.3389/fspas.2021.667058

1 INTRODUCTION

Response of nuclei to incoming neutrinos is categorized into two types of reactions: charged-current (CC) and neutral-current (NC). Gamow-Teller (GT) transition of nuclei belongs to the CC neutrino reaction, while the isovector (IV) spin magnetic-dipole ($M1$) transition to NC. The GT ($\Delta J^\pi = 1^+$, $\Delta T = 1$ and $\Delta T_z = \pm 1$) transitions are analogous to the IV spin-$M1$ ($\Delta J^\pi = 1^+$, $\Delta T = 1$ and $\Delta T_z = 0$) transitions under isospin symmetry. Relevant transition rates are predicted by theoretical models such as the shell-model. The experimentally observed transition rates are, however, quenched compared to the model predictions by employing bare transition operators. Quenching is a basic property of nuclear structure and influences the neutrino reaction rates in astrophysical processes and terrestrial neutrino detectors. The nuclear spin responses and their quenching have strong effects on the mean free path of neutrinos in dense nuclear matter, the size of the neutrino sphere formed in the center of a core-collapsing star, and the cooling process of proton-neutron stars.

The quenching has been extensively studied for the GT transitions. The GT transition strength contained in the GT giant resonances studied by (p, n) reactions was found to be ~60% of the prediction by the Ikeda-Fujii-Fujita sum-rule (Ikeda et al., 1963) consistently for a large variety of nuclei. Two mechanisms were presented to explain GT quenching in the context of the mixing of higher-order configurations with the fundamental one-particle-one-hole nature of the GT excitation. One is the Δ-hole mixing originating from the quark degree of freedom. The other is the two-particle-two-hole as well as the higher-order particle-hole excitations within the nucleonic degree of freedom. Detailed study of the GT strength distribution embedded in the continuum located above the GT giant resonance revealed that the major part of quenching is caused by mixing in the nucleonic degree of freedom (Ichimura et al., 2006). The observed GT transition strengths studied by beta-decay are also quenched from shell-model predictions using the bare g-factor. Recent ab initio calculations using the chiral effective field theory (Gysbers et al., 2019) indicated that quenching was resolved by introducing two-body currents and nuclear many-body correlations. Quenching in the analogous spin-$M1$ transitions was studied by proton inelastic scattering (Anantaraman et al., 1984; Crawley et al., 1989). The result was unclear due to the poor quality of the experimental data and to the ambiguity of the transition matrix element relying on the reaction calculation. This problem has been overcome by the achievement of a high-precision measurement (Matsubara et al., 2015) using high-resolution proton scattering at forward scattering angles including zero degrees that reported the quenching of the nuclear matrix elements for the IV spin-$M1$ transitions, similar to the analogous GT transitions, but no-quenching for the isoscalar (IS) spin-$M1$. Exhaustion of the sum-rule of the spin-$M1$ strengths is relevant to the spin susceptibility of asymmetric nuclear matter, its response to the strong magnetic field in magnetars, and possible phase-transition of nuclear medium in a neutron star to the ferromagnetic state.

The experimental work gave new insight, by the use of the non-energy-weighted sum-rule, that the underlying quenching mechanism is embedded in the ground state property as spin-spin correlation of neutron(n)-proton(p) pairs. The expectation value of the correlation in the ground state is equivalent to the difference of the quenching of nuclear matrix elements between the IS and IV spin-$M1$ transitions. Thus, the quenching of the IS and IV spin-$M1$ transitions needs to be described simultaneously and mutually-consistently. The details are described in **Section 5.4**.

The n-p correlation in the nuclear ground state is one of the recent topics in nuclear physics. The short range correlation as well as the tensor correlation are considered to be the origin of the neutron-proton correlation and are relevant to the IS spin-triplet n-p pairing. The high-momentum nature of the correlation has been studied by the knockout reaction by electron scattering (Subedi et al., 2008; Hen et al., 2014; Hen et al., 2017) or by high-momentum transfer reaction by using (p, d) scattering (Ong et al., 2013; Terashima et al., 2018). In both cases, dominant contribution of the n-p pairs is reported rather than the identical pairs, n-n or p-p, to the high-momentum component in the ground state.

In a different approach, the spin-aligned IS n-p coupling of the valence particles around the Fermi surface was studied from a level structure determined by gamma spectroscopy (Cederwall et al., 2011). It is interesting to observe how those n-p paring components and the IS spin-triplet n-p pairing are related to the n-p spin-spin correlation in the ground state.

In the work of Matsubara et al. (2015), IS and IV spin-$M1$ excitation strength distributions were individually determined by a high-resolution proton inelastic scattering experiment at zero degrees and forward angles for self-conjugate even-even nuclei from ^{12}C to ^{36}Ar. The squared nuclear matrix element of each transition was extracted from the observed differential cross-section by using the unit cross-section method. The summed strength up to the excitation energy of 16 MeV was compared with the prediction by a shell-model for the discussion of quenching of the IS and IV transitions. In this article we describe in greater detail the unit cross-section method in the data analysis. Also, the observed no-quenching of the IS spin-M1 transitions is compared with the historical knowledge of the quenching of the IS magnetic moment. The difference of IS and IV quenching is discussed in terms of the n-p spin-spin correlation in the ground state.

In **Section 2**, formalism is presented for discussion of the nuclear matrix elements of the IS and IV spin-$M1$ transitions, the IS and IV magnetic moments of the nuclear ground state, sum-rules, and the n-p spin-spin correlation function. The experimental methods and the data analysis are described in **Section 3**. The nuclear matrix elements are determined from the experimental data by using the unit cross-section method as described in **Section 4**. The quenching of the IS and IV spin-$M1$ nuclear matrix elements, IS magnetic moment, and the n-p spin-spin correlation are discussed in **Section 5**. Summary and prospects are given in **Section 6**.

2 FORMALISM

2.1 Nuclear Magnetic Moment

The $M1$ operator $\hat{O}(M1)$ for magnetic dipole moments and $M1$ transitions consists of an orbital part ($\vec{l}$) and a spin part ($\vec{s}$).

$$\hat{O}(M1) = \left[\sum_{k=1}^{Z}\left(g_l^{\pi}\vec{l}_k + g_s^{\pi}\vec{s}_k\right) + \sum_{k=Z+1}^{A}\left(g_l^{\nu}\vec{l}_k + g_s^{\nu}\vec{s}_k\right)\right]\mu_N \quad (1)$$

$$= \left[\sum_{k=1}^{A}\left\{\left(g_l^{\mathrm{IS}}\vec{l}_k + g_s^{\mathrm{IS}}\frac{\vec{\sigma}_k}{2}\right) + \left(g_l^{\mathrm{IV}}\vec{l}_k + g_s^{\mathrm{IV}}\frac{\vec{\sigma}_k}{2}\right)\vec{\tau}_{z,k}\right\}\right]\mu_N, \quad (2)$$

where μ_N is the nuclear magneton, $\vec{\sigma}$ is the Pauli spin matrix, the operator $\vec{\tau}_{z,k}$ is the third component of the isospin operator $\vec{\tau}$ acting on the k-th nucleon and its eigen value is +1 for neutrons (ν) and −1 for protons (π). The gyromagnetic factors (g-factors) of g_l^{IS}, g_s^{IS}, g_l^{IV}, and g_s^{IV} are taken as $g_l^{\mathrm{IS}} = \frac{1}{2}(g_l^{\pi} + g_l^{\nu}) = 0.5$, $g_s^{\mathrm{IS}} = \frac{1}{2}(g_s^{\pi} + g_s^{\nu}) = 0.880$, $g_l^{\mathrm{IV}} = -\frac{1}{2}(g_l^{\pi} - g_l^{\nu}) = -0.5$, and $g_s^{\mathrm{IV}} = -\frac{1}{2}(g_s^{\pi} - g_s^{\nu}) = -4.706$, where the g-factors in the free space, $g_l^{\pi} = 1$, $g_l^{\nu} = 0$, $g_s^{\pi} = 5.586$, and $g_s^{\nu} = -3.826$, are employed. The

suffixes of IS and IV denote isoscalar and isovector, respectively. Thus, a magnetic moment is expressed as

$$\mu = \langle i|\widehat{O}(M1)|i\rangle_{M=J}, \tag{3}$$

where $|i\rangle$ denotes an initial state. Here, magnetic moments can be divided into IS and IV parts by corresponding analogous magnetic moments in mirror nuclei ($T_z = \pm T$) as

$$\mu_{\rm IS} = \frac{1}{2}(\mu_+ + \mu_-) \tag{4}$$

$$\mu_{\rm IV} = \frac{1}{2}(\mu_+ - \mu_-), \tag{5}$$

respectively, where $\mu_{+(-)}$ is a magnetic moment in the case of $T_z = +T(-T)$. Because total spin has a relation $J = l + s$, the following can be obtained

$$J = \langle i|L_z|i\rangle_{M=J} + \langle i|S_z|i\rangle_{M=J}, \tag{6}$$

where $L = \sum_k^A \vec{l}_k$ and $S = \sum_k^A \vec{s}_k$ (Brown and Wildenthal, 1983). Applying the above relation to IS magnetic moment ($\mu_{\rm IS} = \langle i|g_l^{\rm IS}L + g_s^{\rm IS}S|i\rangle_{M=J}$), one gets

$$\langle S\rangle \equiv \langle i|S_z|i\rangle_{M=J} = \frac{\mu_{\rm IS} - g_l^{\rm IS}\times J}{g_s^{\rm IS} - g_l^{\rm IS}}, \tag{7}$$

where we denote the function as $\langle S\rangle$ according to Brown and Wildenthal (1983), and it will be discussed in **Section 5.3**.

2.2 M1 Transition Strength

The reduced transition probability (transition strength) for $M1$ excitation is written as

$$\begin{aligned} B(M1) &= \frac{3}{4\pi}\left|\langle f\|\widehat{O}(M1)\|i\rangle\right|^2 \\ &= \frac{3}{4\pi}\left|g_l^{\rm IS}M_{\rm f}\left(\vec{l}\right) + \frac{g_s^{\rm IS}}{2}M_{\rm f}\left(\vec{\sigma}\right) + g_l^{\rm IV}M_{\rm f}\left(\vec{l}\,\tau_z\right)\right. \\ &\quad \left. + \frac{g_s^{\rm IV}}{2}M_{\rm f}\left(\vec{\sigma}\,\tau_z\right)\right|^2\mu_N^2, \end{aligned} \tag{8}$$

where $|f\rangle$ denotes a final state in a transition. Following the convention of Edmonds (Edmonds, 1960; Brown and Wildenthal, 1987), the reduced nuclear matrix element in spin from an initial state to a final state is defined as

$$M_{\rm f}\left(\widehat{O}\right) = \frac{1}{\sqrt{2J_i+1}}\left\langle f\left\|\sum_{k=1}^A \widehat{O}_k\right\|i\right\rangle, \tag{9}$$

where $\widehat{O}_{(k)}$ denotes $\vec{l}_{(k)}$, $\vec{\sigma}_{(k)}$, $\vec{l}_{(k)}\tau_{z(,k)}$, and $\vec{\sigma}_{(k)}\tau_{z(,k)}$. Expressing corresponding analogous $M1$ transitions in mirror nuclei ($T_z = \pm T$) as $B(M1)_\pm$, IS and IV parts of a transition strength $B(M1)$ can be written using $B(M1)_\pm$ (Fujita et al., 2000; Fujita et al., 2011) or using the reduced matrix elements as

$$\begin{aligned} B(M1)_{\rm IS} &= \frac{1}{4}\left[\sqrt{B(M1)_+} - \sqrt{B(M1)_-}\right]^2 \\ &= \frac{3}{4\pi}\left|g_l^{\rm IS}M_{\rm f}\left(\vec{l}\right) + \frac{g_s^{\rm IS}}{2}M_{\rm f}\left(\vec{\sigma}\right)\right|^2\mu_N^2 \end{aligned} \tag{10}$$

$$\begin{aligned} B(M1)_{\rm IV} &= \frac{1}{4}\left[\sqrt{B(M1)_+} + \sqrt{B(M1)_-}\right]^2 \\ &= \frac{3}{4\pi}\left|g_l^{\rm IV}M_{\rm f}\left(\vec{l}\,\tau_z\right) + \frac{g_s^{\rm IV}}{2}M_{\rm f}\left(\vec{\sigma}\,\tau_z\right)\right|^2\mu_N^2, \end{aligned} \tag{11}$$

respectively. If only spin parts are extracted as IS and IV spin-$M1$ transition strengths, they are expressed as

$$B(M1)_\sigma = \frac{3}{4\pi}\left|\frac{g_s^{\rm IS}}{2}M_{\rm f}\left(\vec{\sigma}\right)\right|^2\mu_N^2 \tag{12}$$

$$B(M1)_{\sigma\tau} = \frac{3}{4\pi}\left|\frac{g_s^{\rm IV}}{2}M_{\rm f}\left(\vec{\sigma}\,\tau_z\right)\right|^2\mu_N^2 \tag{13}$$

respectively.

Here, we focus on an IS part, $B(M1)_{\rm IS}$. Because total angular momentum operator ($\vec{j} = \vec{l} + \vec{\sigma}/2$) gives a good quantum number, taking a ground state as $|{\rm g.s.}\rangle$, $\vec{j}\,|{\rm g.s}\rangle$ is proportional to $|{\rm g.s}\rangle$ but is orthogonal to any other eigenstates. Thus, the following restriction (Bernabéu et al., 1992; Kawabata et al., 2004) can be obtained

$$\left\langle {\rm f}\left\|\sum_{k=1}^A\left(\vec{l}_k + \frac{1}{2}\vec{\sigma}_k\right)\right\|{\rm g.s.}\right\rangle = 0 \tag{14}$$

Since the above restriction leads to $M_{\rm f}(\vec{l}) = -\frac{1}{2}M_{\rm f}(\vec{\sigma})$, the right-hand side of **Eq. 10** is rewritten as

$$B(M1)_{\rm IS} = \frac{3}{4\pi}\left|\frac{g_s^{\rm IS} - g_l^{\rm IS}}{2}M_{\rm f}\left(\vec{\sigma}\right)\right|^2\mu_N^2 = \left(\frac{g_s^{\rm IS} - g_l^{\rm IS}}{g_s^{\rm IS}}\right)^2 B(M1)_\sigma \tag{15}$$

2.3 Squared Nuclear Matrix Element

Nuclear excitation $\Delta J^\pi = 1^+$ with $\Delta T_z = 0$ is an $M1$ transition. When nuclear excitation at low momentum transfer is considered, spin-parts of the $M1$ transition are probed due to the local nature of the nucleon-nucleon (NN) interaction (Petrovich and Love, 1981). Thus, the 1^+ excitation by (p, p') reaction at forward angles is spin-$M1$ transition. Since spin-$M1$ transition is not probed by electromagnetic interaction but by nuclear interaction, its transition strength does not relate to g-factors. Therefore, transition strengths of IS and IV spin-M1 transitions from the ground state $|{\rm g.s.}\rangle$ to an excited state $|f\rangle$ are expressed by squared nuclear matrix element (SNME) as

$$\left|M_{\rm f}(\vec{\sigma})\right|^2 = \left|\frac{1}{\sqrt{2J_i+1}}\left\langle {\rm f}\left\|\sum_{k=1}^A\vec{\sigma}_k\right\|{\rm g.s.}\right\rangle\right|^2 \tag{16}$$

$$\left|M_{\rm f}(\vec{\sigma}\,\tau_z)\right|^2 = \left|\frac{1}{\sqrt{2J_i+1}}\left\langle {\rm f}\left\|\sum_{k=1}^{\rm A}\vec{\sigma}_k\tau_{z,k}\right\|{\rm g.s.}\right\rangle\right|^2 \tag{17}$$

respectively. The factor $1/\sqrt{2J_i+1}$ is unity for a 0^+ ground state.

2.4 Relation to Gamow-Teller Excitation

Next, reduced nuclear matrix element and transition strength in GT excitation are defined as

$$M_{\rm f}\left(\overrightarrow{\sigma}\tau_{\pm}\right) = \frac{1}{\sqrt{2J_i+1}}\left\langle {\rm f}\left\|\frac{1}{\sqrt{2}}\sum_{k=1}^{A}\overrightarrow{\sigma}_k\tau_{\pm,k}\right\|{\rm g.s.}\right\rangle \tag{18}$$

$$B(GT^{\pm}) = \left|M_{\rm f}\left(\overrightarrow{\sigma}\tau_{\pm}\right)\right|^2, \tag{19}$$

respectively, where $\tau_{\pm} = \frac{1}{2}(\tau_x \pm i\tau_y)$. Applying the Wigner-Eckart theorem in the isospin space, transition strengths of GT and IV spin-$M1$ excitations are obtained as

$$B(GT^{\pm}) = \left|\frac{1}{\sqrt{2J_i+1}}\frac{\langle T_i, T_{iz}, 1, \pm 1|T_f, T_{fz}>}{\sqrt{2T_f+1}}\frac{1}{\sqrt{2}}M'(GT^{\pm})\right|^2, \tag{20}$$

$$B(M1)_{\sigma\tau} = \frac{3}{4\pi}\left|\frac{g_s^{\rm IV}}{2}\frac{1}{\sqrt{2J_i+1}}\frac{\langle T_i, T_{iz}, 1, 0|T_f, T_{fz}\rangle}{\sqrt{2T_f+1}}M'(M1_{\sigma\tau})\right|^2\mu_N^2, \tag{21}$$

respectively, where $M'(GT^{\pm})$ and $M'(M1_{\sigma\tau})$ are reduced nuclear matrix elements in spin and isospin expressed as

$$M'(GT^{\pm}) = \left\langle {\rm f}\left|\left|\sum_{k=1}^{A}\overrightarrow{\sigma}_k\tau_{\pm,k}\right|\right|{\rm g.s.}\right\rangle \tag{22}$$

$$M'(M1_{\sigma\tau}) = \left\langle {\rm f}\left|\left|\sum_{k=1}^{A}\overrightarrow{\sigma}_k\tau_{z,k}\right|\right|{\rm g.s.}\right\rangle \tag{23}$$

respectively. Because $|M'(GT^{\pm})|^2 = |M'(M1_{\sigma\tau})|^2$ is realized under the assumption of isospin symmetry, the following relationship between $B(GT^{\pm})$ and $B(M1)_{\sigma\tau}$ can be obtained as

$$\frac{B({\rm GT}^{\pm})}{B(M1)_{\sigma\tau}/\mu_N^2} = \frac{8\pi}{3}\frac{1}{(g_s^{IV})^2}\frac{\langle T_i, T_{iz}, 1, \pm 1|T_f, T_{fz}\rangle^2}{\langle T_i, T_{iz}, 1, 0|T_f, T_{fz}\rangle^2} \tag{24}$$

Here, it should be noted that the isospin symmetry is reasonably assumed within the accuracy of the data in the present study although the meson exchange current contribution can be different between an IV $M1$ transition measured by electron scattering and the analogous GT transition by charge-exchange reaction (Richter et al., 1990; Lüttge et al., 1996).

2.5 Total Spin Correlation in Ground State

For the discussion of total spin correlation in a ground state (Matsubara et al., 2015), the difference between the sums of the IS and IV spin-$M1$ SNMEs integrated up to the excitation energy of E_x, $\Delta_{\rm spin}(E_x)$, is defined as

$$\Delta_{\rm spin}(E_{\rm x}) = \frac{1}{16}\left\{\sum_{E_{\rm f}<E_{\rm x}}\left|M_{\rm f}(\overrightarrow{\sigma})\right|^2 - \sum_{E_{\rm f}<E_{\rm x}}\left|M_{\rm f}(\overrightarrow{\sigma}\tau_{\rm z})\right|^2\right\}$$

With the proton (neutron) total spin operator $\overrightarrow{S}_{p(n)}$ defined as

$$\overrightarrow{S}_{p(n)} = \frac{1}{2}\sum_{k=1}^{Z(N)}\overrightarrow{\sigma}_k, \tag{26}$$

the sum is taken for all the protons (neutron).When a ground state is $J^{\pi} = 0^+$, the IS and IV spin-$M1$ nuclear matrix elements are represented by

$$M_{\rm f}\left(\overrightarrow{\sigma}\right) = 2\left\langle {\rm f}\left|\overrightarrow{S}_n + \overrightarrow{S}_n\right|0\right\rangle \tag{27}$$

$$M_{\rm f}\left(\overrightarrow{\sigma}\tau_{\rm z}\right) = 2\left\langle {\rm f}\left|\overrightarrow{S}_n - \overrightarrow{S}_p\right|0\right\rangle \tag{28}$$

respectively, where $|0\rangle$ denotes the ground state. In the limit of $E_{\rm x}\rightarrow\infty$, the completeness of the final state, $|{\rm f}\rangle$, yields

$$\left\langle\left(\overrightarrow{S}_n + \overrightarrow{S}_p\right)^2\right\rangle = \sum_{\rm f}\langle {\rm g.s.}\left|\overrightarrow{S}_{\rm n} + \overrightarrow{S}_{\rm p}\right|{\rm f}\rangle\langle {\rm f}\left|\overrightarrow{S}_{\rm n} + \overrightarrow{S}_{\rm p}\right|{\rm g.s.}\rangle = \lim_{E_{\rm x}\rightarrow\infty}\frac{1}{4}\sum_{E_{\rm f}<E_{\rm x}}\left|M_{\rm f}\left(\overrightarrow{\sigma}\right)\right|^2 \tag{29}$$

$$\left\langle\left(\overrightarrow{S}_n - \overrightarrow{S}_p\right)^2\right\rangle = \lim_{E_{\rm x}\rightarrow\infty}\frac{1}{4}\sum_{E_{\rm f}<E_{\rm x}}\left|M_{\rm f}\left(\overrightarrow{\sigma}\tau_{\rm z}\right)\right|^2 \tag{30}$$

Here the expectation values of the left side of the equations are taken for the 0^+ ground state. We then derive

$$\Delta_{\rm spin} \equiv \lim_{E_{\rm x}\rightarrow\infty}\Delta_{\rm spin}(E_{\rm x}) = \frac{1}{4}\left\{\left\langle\left(\overrightarrow{S}_n + \overrightarrow{S}_p\right)^2 - \left(\overrightarrow{S}_n - \overrightarrow{S}_p\right)^2\right\rangle\right\} = \langle\overrightarrow{S}_p\cdot\overrightarrow{S}_n\rangle \tag{31}$$

which represents the expectation value of the proton-neutron spin-spin correlation in the ground state.

3 EXPERIMENT

In this section we briefly describe the experimental method and the assignment of the spin-M1 excitations. Details can be found in former publications (Tamii et al., 2009; Matsubara et al., 2015; von Neumann-Cosel and Tamii, 2019).

3.1 Measurement of the (*p,p'*) Reactions

The experiment was performed at the cyclotron facility of the Research Center for Nuclear Physics (RCNP), Osaka University. A proton beam was accelerated by a cascade of two cyclotrons to $E_{\rm p}$ = 295 MeV. The beam was transported to the West-South (WS) beam line (Wakasa et al., 2002), where a high-dispersion on target was created. An excitation-energy resolution of 18 keV (FWHM) was achieved by applying dispersion matching (Fujita et al., 1997; Fujita H. et al., 2002; Fujita et al., 2011) between the WS beam line and the Grand Raiden (GR) spectrometer (Fujiwara et al., 1999). The scattered protons by the target were momentum-analyzed and were detected by two sets of multi-wire drift-chambers and two plastic scintillation counters at the focal plane by GR spectrometer. A scattering angle range of 0–14° was covered by placing the GR spectrometer at 0, 2.5, 4.5, 6, 8, 10, 12, and 14°. The details of the experimental technique are described in Ref. (Tamii et al., 2009; von Neumann-Cosel and Tamii, 2019).

Self-conjugate even-even nuclei, ^{12}C, ^{24}Mg, ^{28}Si, ^{32}S and ^{36}Ar, were used as the target. Areal densities of 1.0–2.5 mg/cm^2 were prepared for ^{12}C, ^{24}Mg, and ^{28}Si. Magnesium and argon targets were isotopically enriched to 100%, while the others were in

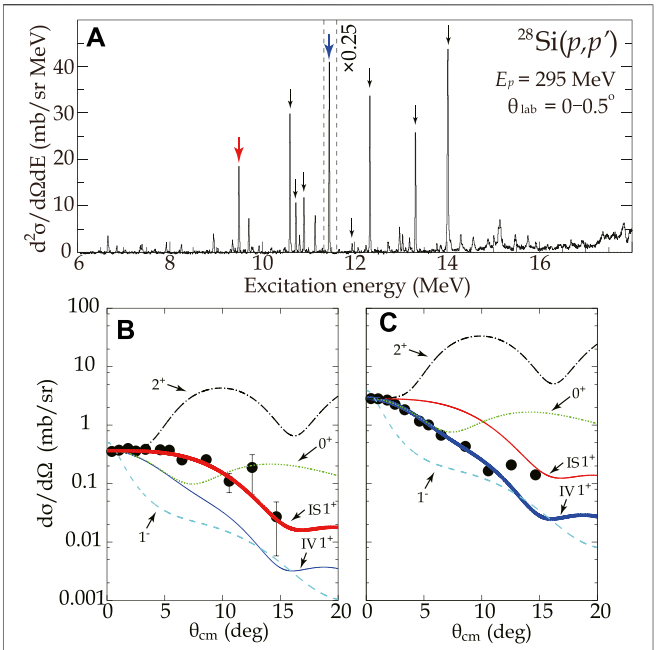

FIGURE 1 | (A) Excitation energy spectrum of the ^{28}Si(p,p') reaction at E_p = 295 MeV and θ_{lab} = 0° – 0.5°. The arrows in the figure indicate conditions that are definitely determined as 1$^+$. Angular distributions of **(B)** IS and **(C)** IV spin-M1 excitations marked by red and blue arrows in **(A)**, respectively, in comparison with theoretical angular distributions for several multipolarities. The figures were taken from Matsubara et al. (2015).

natural abundance. The ^{32}S target was kept at the liquid nitrogen temperature for preventing sublimation due to heat by charged particle irradiation (Matsubara et al., 2009) with an areal density of 15 mg/cm^2. The ^{36}Ar target was kept at 1.0 atm in a gas cell at room temperature (Matsubara et al., 2012) sealed by aramid foils with a thickness of 6 μm on one side.

3.2 Assignment of Spin-M1 Excitations

Figure 1A shows an excitation energy spectrum of the ^{28}Si(p, p') reaction at a scattering angle of 0.0–0.5°. The excited states below E_x = 16 MeV are well isolated from the others. Excited state with a spin-parity of 1$^+$ state was identified by comparing the shape of the measured angular distribution of the differential cross-section with Distorted-Wave Impulse Approximation (DWIA) calculations by using the code DWBA07 (Raynal, 2007). One-body transition densities were obtained by shell-model calculations with the code Nushell@MSU (Brown and Rae, 2014) and the USD interactions (Brown and Wildenthal, 1983). No sizable difference in the angular distribution was observed depending on the choice of the effective interaction from USD, USDA, or USDB (Brown and Richter, 2006; Richter et al., 2008). The effective *NN* interaction parametrized at 325 MeV was used after conversion to a beam energy of 295 MeV as indicated in (Love and Franey, 1981; Franey and Love, 1985). Optical potential parameters were determined by fitting the angular distribution of the differential cross-section of the elastic scattering measured in the same experiment (Matsubara, 2010). Harmonic oscillator parameters were taken from a global analysis (Kirson, 2007).

The measured angular distributions of the differential cross-section for the excited states at E_x = 9.495 (1$^+$: T = 0) and 11.447 MeV (1$^+$: T = 1) in ^{28}Si are shown in **Figures 1B,C**, respectively, by the solid circles. They are compared with the predictions of the DWIA calculation shown by the curves for J^π = 0$^+$, 1$^-$, and 2$^+$, and for each of the IS and IV 1$^+$ transitions. The predicted cross-sections are normalized to the experimental data at the smallest measured angle. The angular distribution of the IS 1$^+$ excitation is predicted to be flatter than the IV 1$^+$ excitation at the forward angles smaller than 5° due to the relatively stronger contribution of the exchange tensor component compared to the central component in the effective *NN* interaction (Franey and Love, 1985; Tamii et al., 1999). Thus, the measured angular distribution allowed determination of the transferred isospin, ΔT = 0 (IS) or 1 (IV), for the 1$^+$ transitions.

The IS and IV 1$^+$ excited states were assigned from the observed discrete excited states by the following method. First the angular distribution of the differential cross-sections for each of the observed discrete excited states was deduced from the data analysis. The excited states were selected according to the angular distribution below 5° for those having an almost flat distribution as a signature of an IS 1$^+$ state or a quickly dropping distribution of an IV 1$^+$ state as shown in **Figures 1B,C**, respectively. Second, the most appropriate assignment was chosen from IS 1$^+$, IV 1$^+$, 0$^+$, 1$^-$, and 2$^+$ distributions by comparing the angular distribution up to 14° with the theoretical predictions. Third, the assignment for the IS or IV 1$^+$ states with a reduced χ^2 value close to unity was taken as confident and that for the rests as less confident. The confident assignments of the IS and IV 1$^+$ states were in good agreement for the conditions studied by electron scattering (Bendel et al., 1971; Richter et al., 1990; Foltz et al., 1994; Lüttge et al., 1996; Hofmann et al., 2002). The high energy-resolution measurement allowed us to observe several new states including the less-confident assignments as shown in **Section 5.1**.

4 UNIT CROSS-SECTION METHOD

4.1 Definition

4.1.1 Unit Cross-Section

The differential cross-section of the 1$^+$ excitations by proton inelastic scattering at 0° is considered to be approximately proportional to SNME in the intermediate energy region of 100–400 MeV. Unit cross-sections (UCSs), $\hat{\sigma}_{IS}$ and $\hat{\sigma}_{IV}$, are introduced in analogy to the study of Gamow-Teller excitations by (p, n) reactions (Taddeucci et al., 1987; Sasano et al., 2009). The differential cross-section at 0° is written as

$$\frac{d\sigma}{d\Omega}(0^\circ) = \hat{\sigma}_T F_T(q, E_x)\left|M_f(\mathcal{O}_T)\right|^2 \quad (32)$$

where T stands for IS or IV. $\mathcal{O}_T$ is the operator, $\vec{\sigma}$ or $\vec{\sigma}\tau_z$, for IS or IV transitions, respectively. $F_T(q, E_x)$ is the kinematic factor that accounts for dependence on the momentum transfer (q) and the excitation energy (E_x), and was determined by the DWIA

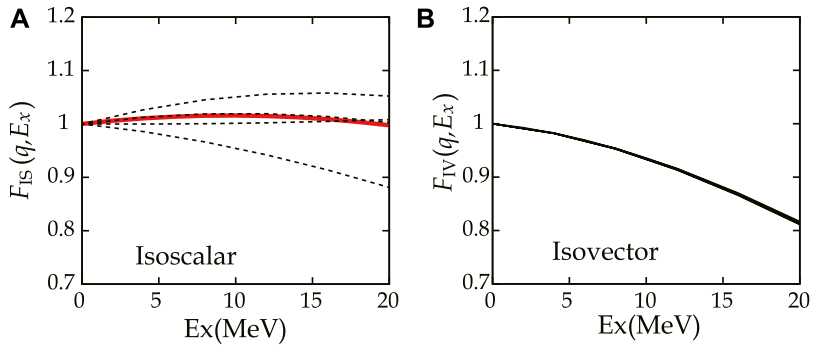

FIGURE 2 | Kinematic correction factors $F_{\mathrm{IS}}(q,E_x)$ and $F_{\mathrm{IV}}(q,E_x)$ in the case of ^{28}Si obtained from DWIA calculation using USD interaction. **(A)** The strongest excitation and others are drawn in red bold and black dashed curves, respectively. **(B)** Distributions of several IV OBTDs are overlapped.

TABLE 1 | Data used for obtaining IV UCSs.

Nuclide	E_x (MeV)	$\frac{d\sigma}{d\Omega}$ (0.4°) (mb/sr)	$F_{\mathrm{IV}}(q,E_x)$	$B(\mathrm{GT}^{\pm})$	$\hat{\sigma}_{\mathrm{IV}}$ (mb/sr)
^{12}C	15.113	3.429 ± 0.62	0.897	0.924 ± 0.04	2.11 ± 0.13
^{26}Mg	13.302	0.703 ± 0.30	0.904	0.408 ± 0.018	1.92 ± 0.12
^{58}Ni	10.655	0.981 ± 0.12	0.916	0.191 ± 0.022	0.94 ± 0.11

calculation as explained in **Section 4.1.2**. The target mass (A) dependence of UCSs is parameterized as (Taddeucci et al., 1987)

$$\hat{\sigma}_T(A) = N_T \exp\left(-x_T A^{1/3}\right) \tag{33}$$

where N_T and x_T are the normalization and mass-dependence parameters. The mass-dependence parameter x_T essentially originates from the distortion effect of the reaction that is common between the IS and IV transitions. Thus we assume $x_{IS} = x_{IV}$, which is held within an accuracy of 5% in DWIA calculations. Details will be discussed in **Section 4.4.2**.

4.1.2 Kinematic Factor

The kinematic factors $F_{\mathrm{IS}}(q,E_x)$ and $F_{\mathrm{IV}}(q,E_x)$ were determined by DWIA calculation using the USD interaction as shown in **Figure 2** as a case of ^{28}Si, where only OBTDs above the experimental detection limit were employed. The distributions were obtained from a ratio of differential cross-section at 0° at $E_x \neq 0$ to that at $E_x = 0$. As seen in **Figure 2B**, IV distributions of the kinematic factor overlap. Since the result suggests that $F_{\mathrm{IV}}(q,E_x)$ does not depend on wavefunction, $F_{\mathrm{IV}}(q,E_x)$ was expressed as a smooth function of E_x and A by fitting. As shown in **Figure 2A**, however, IS distributions of the kinematic factor depend on wavefunction as they do not overlap. Because the result suggests that $F_{\mathrm{IS}}(q,E_x)$ cannot be expressed as a function of E_x owing to dependence of wavefunction, $F_{\mathrm{IS}}(q,E_x) = 1.00 \pm 0.10$ was simply assumed in order to cover the variation of wavefunctions below $E_x = 15$ MeV.

4.2 Derivation From Experiment

4.2.1 Cases of 12-Carbon, 26-Magnesium, 58-Nickel

Isovector UCSs of ^{12}C, ^{26}Mg, and ^{58}Ni were obtained using the data summarized in **Table 1** by assuming isospin symmetry. The

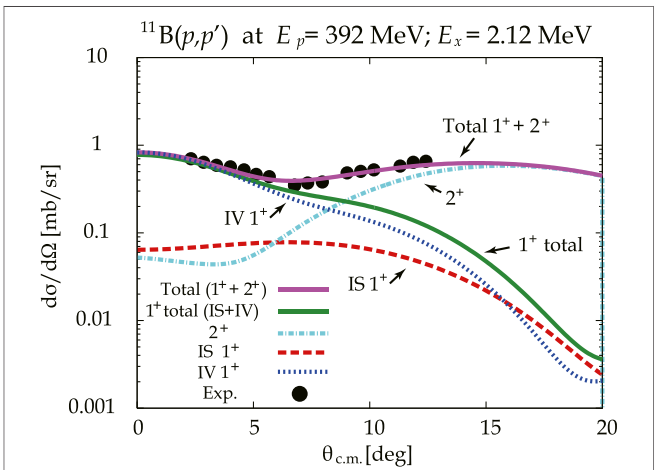

FIGURE 3 | Decomposition of differential cross-section of ^{11}B(p,p') reaction at E_p = 392 MeV compared to the state at E_x = 2.12 MeV. The experimental data were taken from Kawabata et al. (2004).

differential cross-section of (p,p') reaction at E_p = 295 MeV at scattering angles 0.4° was taken from Tamii et al. (2009), where 0.4° is the most forward angle by selecting scattering angles between 0.0 and 0.5°. The cross-section was extrapolated to E_x = 0 MeV using $F_{\mathrm{IV}}(q,E_X)$.

Log ft-value of β-decay and (^{3}He, t) data (Alburger and Nathan, 1978; Fujita Y. et al., 2002; Zegers et al., 2006; Fujita et al., 2007; Fujita et al., 2011) were used to obtain GT strength ($B(\mathrm{GT}^{\pm})$) from ground state to an excited state corresponding to the (p,p') cross-section under the isospin symmetry. After $B(\mathrm{GT}^{\pm})$ was converted to IV spin-$M1$ SNME following **Eqs. 13**, **24**, $\hat{\sigma}_{\mathrm{IV}}$ was obtained. Here, the (p,n) data (Sasano et al., 2009) were also employed for the calibration of $B(\mathrm{GT}^{-})$ in ^{58}Ni.

4.2.2 Case of 11-Boron

The γ-decay widths of the mirror states in ^{11}B and ^{11}C from the first excited states (Firestone, 1996), corresponding to $B(M1)_{11\mathrm{B}}$ and $B(M1)_{11\mathrm{C}}$, respectively, were employed to obtain $B(M1)_{\mathrm{IS}}$ and $B(M1)_{\mathrm{IV}}$ following **Eqs. 10**, **11**. Then, $B(M1)_{\sigma}$ and $B(M1)_{\sigma\tau}$

TABLE 2 | Data used for obtaining UCSs of ^{11}B. The upper table is expressed in unit of μ_N^2.

$B(M1)_{11_B}$	$B(M1)_{11_C}$	$B(M1)_{IS}$	$B(M1)_{IV}$	$B(M1)_{\sigma}$	$B(M1)_{\sigma\tau}$
0.544 ± 0.043	0.347 ± 0.024	0.0055 ± 0.0013	0.440 ± 0.012	0.030 ± 0.007	0.57 ± 0.04
$\frac{d\sigma}{d\Omega}$ (0°)	392 MeV Kawabata et al. (2004)			295 MeV Tamii et al. (1999), Tamii et al. (2009)	
	Total ($1^+ + 2^+$)	IS 1^+	IV 1^+	IS 1^+	IV 1^+
(mb/sr)	0.820	0.0633	0.818	0.0621 ± 0.0052	0.780 ± 0.042
Nuclide	E_x (MeV)	$F_{IS}(q=0,E_x)$	$\hat{\sigma}_{IS}$ (mb/sr)	$F_{IV}(q=0,E_x)$	$\hat{\sigma}_{IV}$ (mb/sr)
^{11}B	2.12	1.00 ± 0.10	0.0971 ± 0.025	0.9926	1.81 ± 0.16

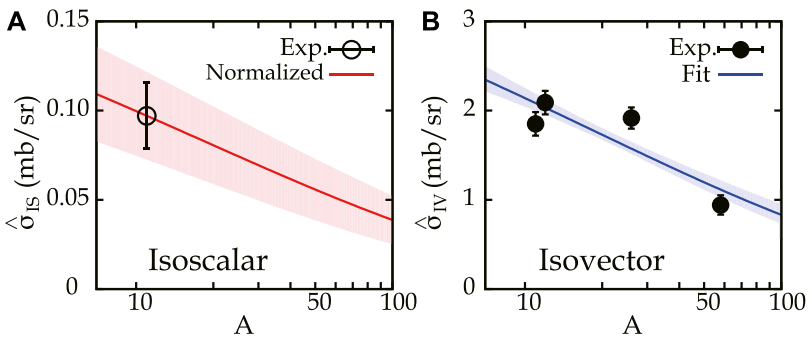

FIGURE 4 | Empirically determined IS **(left)** and IV **(right)** UCSs. The mass dependence of the data were fit with the functional form of **Eq. 33** as shown by the solid lines in the IV panel. The band shows the uncertainty of one sigma. The IS slope parameter x_{IS} is taken to be the same as x_{IV}. The figures were adapted from Matsubara et al. (2015).

were obtained from $B(M1)_{IS}$ and $B(GT^-) = 0.402 \pm 0.031$ (Taddeucci et al., 1990; Kawabata et al., 2004) using **Eqs. 15**, **24**, respectively. Finally, IS and IV spin-$M1$ SNMEs in the case of ^{11}B were obtained using **Eqs. 12**, **13**, respectively.

The differential cross-section data of the ^{11}B(p,p') reaction at E_p = 392 MeV and at E_x = 2.12 MeV was taken from Kawabata et al. (2004). The angular distribution of the differential cross-section was decomposed into IS 1^+, IV 1^+, and 2^+ transitions using the DWIA calculation, where an incoherent (a coherent) sum was assumed between 1^+ and 2^+ (IS 1^+ and IV 1^+) excitations. The OBTDs based on CKPOT interaction (Cohen and Kurath, 1965), the effective *NN* interaction derived at 325 MeV (Love and Franey, 1981; Franey and Love, 1985), and the global optical potential parameters (Cooper et al., 2009) were employed in this calculation. The OBTDs were normalized to reproduce the experimental values of IS and IV SNMEs, and $B(E2)$ (Firestone, 1996) in IS 1^+, IV 1^+, and 2^+ excitations, respectively. Because the normalized OBTDs did not reproduce the experimental angular distribution of the differential cross-section, additional normalization factors of 1.1 and 1.3 were applied to the 1^+ and 2^+ excitations, respectively, as shown in **Figure 3**. The differential cross-section data of total, IS 1^+, and IV 1^+ at E_p = 392 MeV and at 0° were decomposed as summarized in **Table 2**, where the experimental uncertainty was assumed to be negligible because the error bars were invisible in Kawabata et al. (2004). Here, choice of an interaction with OBTDs did not change the final result because differences among CKPOT, SFO (Suzuki et al., 2003), and MK3w (Warburton and Millener, 1989) interactions in the model spaces of *p*, *psd*, and *spsdpf*, respectively, were within 0.5%. Next, the cross-section data at E_p = 392 MeV were converted to those at E_p = 295 MeV by making use of a ratio of the ^{12}C(p,p') reaction at 0° to the states E_x = 12.71 and 15.11 MeV known as IS 1^+ and IV 1^+ excitations, respectively, where the experimental data were taken from Tamii et al. (1999), Tamii et al. (2009). Thus, the data of ^{11}B(p,p') excitation to E_x = 2.12 MeV at E_p = 295 MeV and at 0° were obtained.

Combining the SNMEs with the differential cross-section after correction of $F_T(q,E_x)$, IS and IV UCSs in the case of ^{11}B were obtained as summarized in **Table 2**. Here, $\hat{\sigma}_{IS}$ does not include uncertainty owing to $F_{IS}(q,E_x)$.

TABLE 3 | Empirically determined UCS parameters from the fit shown in **Figure 4**.

N_{IS} (mb/sr)	N_{IV} (mb/sr)	$x_{IV} = x_{IS}$
0.226 ± 0.043	4.85 ± 0.82	0.38 ± 0.06

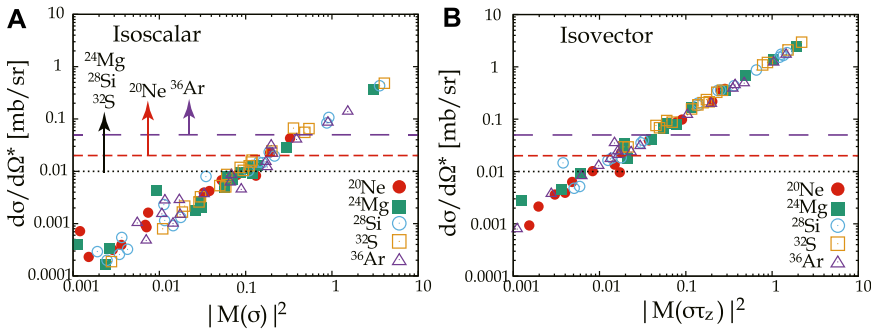

FIGURE 5 | Proportionality of UCS. Horizontal lines indicate experimental detection limit for ^{24}Mg, ^{28}Si and ^{32}S (dotted), ^{20}Ne (short-dashed) and ^{36}Ar (long-dashed). Cross-section is corrected in terms of mass dependence as in **Eq. 34**.

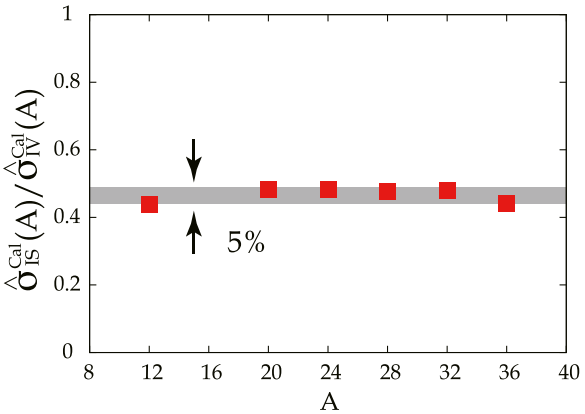

FIGURE 6 | Mass dependence of ratio of IS to IV UCSs studied by calculation.

4.3 Results of Unit Cross-Section

The experimentally obtained IS and IV UCSs were plotted as a function of the mass number in **Figures 4A,B**, respectively. The mass dependence of the IV UCS data was fitted with the functional form of **Eq. 33** having free parameters of N_{IV} and x_{IV}. The result is shown by the solid line in **Figure 4B** with the one-sigma uncertainty band. The IS normalization parameter, N_{IS}, was determined from the data at A = 11. The IS slope parameter, x_{IS}, was taken to be the same as x_{IV} as discussed in **Section 4.4.2**. The IS uncertainty band includes contribution of 10% from the $F_{IS}(q, E_x)$ (**Section 4.1.2**). The obtained parameters are summarized in **Table 3**.

4.4 Model Study

4.4.1 Proportionality of Squared Nuclear Matrix Elements to the Differential Cross-Section

Validity of the application of the UCS method has been theoretically examined by the use of shell-model target wave functions as USD interaction and DWIA calculation. Since $B(M1)_\sigma$ and $B(M1)_{\sigma\tau}$ were calculated using the code Nushell@MSU (Brown and Rae, 2014), SNMEs were obtained from the relations in **Eqs. 12**, **13**. Each differential cross-section at $q = 0$ and at $E_x = 0$ MeV was calculated using corresponding OBTD of the USD interaction. Here the following correction for mass dependence to be normalized to A = 28 was applied as

$$\frac{d\sigma^*}{d\Omega} = \frac{d\sigma}{d\Omega} \times e^{-0.38\times\left(28^{1/3}-A^{1/3}\right)} \tag{34}$$

where $\frac{d\sigma}{d\Omega}^*$ is the corrected cross-section and 0.38 comes from x_T determined in **Table 3**. As shown in **Figure 5**, good linearity was seen especially above the experimental detection limit shown by the lines for each target nucleus.

4.4.2 Distortion Effect

The mass-dependence term in **Eq. 32**, x_T, essentially originates from the distortion effect that is common between the IS and IV transitions. A slope for each nucleus in **Figure 5** corresponds to UCSs theoretically obtained, where the weighting sum within the experimental detection limit was taken. Those ratios of IS to IV UCSs for each nucleus are plotted as a function of mass number in **Figure 6**, where the suffix of "cal" indicates that the value of UCS is obtained from the calculation. The result for ^{12}C is added in **Figure 6**. The SFO interaction (Suzuki et al., 2003), which is applicable to the p-shell nuclei, is used instead of the USD interaction. The results suggest that the assumption is supported, as the ratios are constant within 5%.

5 RESULTS AND DISCUSSION

5.1 Strength Distribution

The SNMEs of the transitions to the excited states assigned as T = 0 (IS) or T = 1 (IV) 1^+ states were determined by using **Eq. 32** from the measured differential cross-section at 0°. The results are plotted in **Figure 7** , where the figure was taken from Matsubara et al. (2015) with addition of the ^{12}C data. The strengths of ^{12}C were observed to be centered to single state, which was consistent with previous work (von Neumann-Cosel et al., 2000). For ^{24}Mg, ^{28}Si, ^{32}S, and ^{36}Ar, we

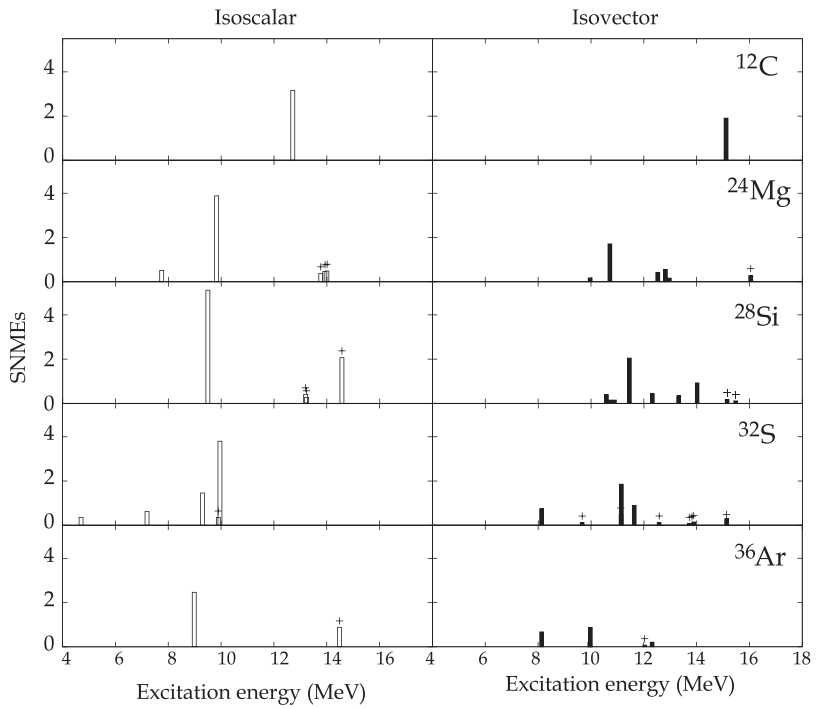

FIGURE 7 | Observed distributions of spin-*M*1 SNMEs. The bars labeled + indicate states with a less confident spin assignment. The figures were taken from Matsubara et al. (2015) with ^{12}C data added.

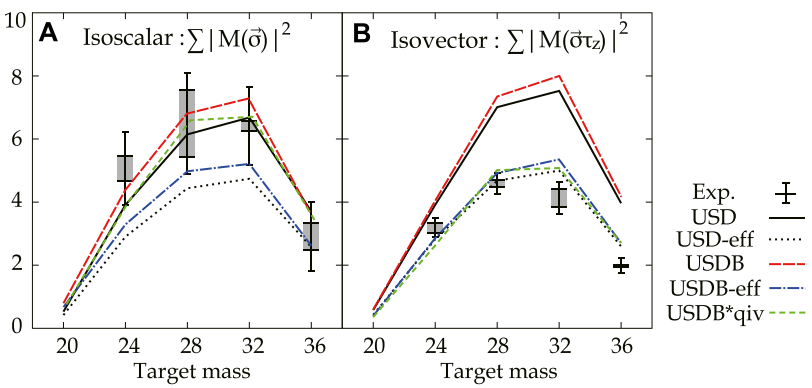

FIGURE 8 | Integrated values of spin-*M*1 SNMEs for IS **(A)** and IV **(B)** transitions up to E_x = 16 MeV as a function of the target mass. Error bars indicate the total experimental uncertainties, and gray bands show partial uncertainties from indefinite spin assignments. Solid and long-dashed lines indicate the prediction of a shell-model calculation using bare USD and bare USDB interactions, respectively. Dotted and dashed-dotted lines applied empirical quenching factors (see text for more details) to USD and USDB interactions, respectively. The short-dashed lines (green) are calculated using the USDB interaction modification in the IS spin-triplet interaction and in the IV quenching factor from Sagawa and Suzuki (2018). The figures were taken from Matsubara et al. (2015) with some updates using the modified interactions (Sagawa and Suzuki, 2018).

identified 1–4 (4–8) states in each target nucleus corresponding to the IS (IV) spin-*M*1 transitions.

Additionally, 1–3 (1–7) states were assigned as IS (IV) spin-*M*1 transitions with less confidence, and they are marked with "+." We reassigned 1–6 states as 0^+, which were claimed as 1^+ in previous studies (Anantaraman et al., 1984; Crawley et al., 1989).

5.2 Quenching of Squared Nuclear Matrix Elements of Isoscalar and Isovector Spin-M1 Transitions

The integrated values of the SNMEs up to E_x = 16 MeV were plotted as a function of the target mass in **Figure 8** for each of the IS (left panel) and IV (right panel) transitions. Error bars show

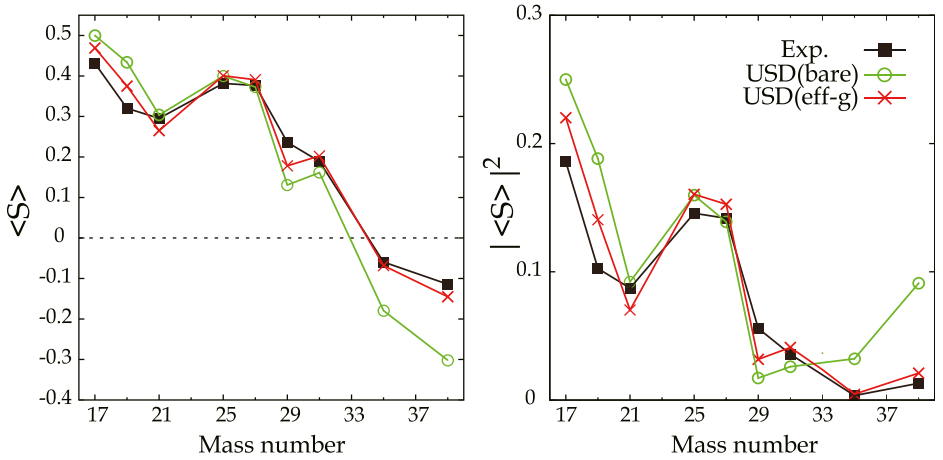

FIGURE 9 | The diagonal spin matrix element $\langle S \rangle$ obtained from the IS magnetic moments of mirror nuclei in the sd-shell region. The data were taken and calculated from Brown and Wildenthal (1983), Brown and Wildenthal (1987). The lines are for guiding the viewer's eyes.

the full experimental uncertainties, while gray bands show the partial uncertainties originating from the less-confident spin-parity assignment of the transitions (see **Section 5.1**). Predicted SNMEs by shell-model calculation employing USD interaction (Brown and Wildenthal, 1987) integrated up to 16 MeV is shown by solid lines. Altering the effective interaction to USDA or USDB (Brown and Richter, 2006; Richter et al., 2008) gave only a small change in the prediction (<10%), as shown in **Figure 8** for USDB (dashed line). It has been found that the measured values are significantly smaller than the model prediction for the integrated IV SNMEs, while the values are consistent with the model prediction of the integrated IS SNMEs within the experimental uncertainties. We defined the quenching factor as the ratio of the experimentally observed SNMEs integrated up to the experimental limit of 16 MeV to the theoretical predictions integrated to the same excitation energy. The numbers are 1.01(9) and 0.61(6), compared with predictions by the shell model using the USD interaction for the IS and IV spin-$M1$ transitions, respectively, when the averages of the measured nuclei are used.

The observed quenching factor of the IV spin-$M1$ transitions is similar to the study of the quenching of the Gamow Teller transitions that is analogous to the IV spin-$M1$ transitions in terms of isospin symmetry (Anderson et al., 1987). Quenching of the reduced transition probability $B(M1)$ is, in a conventional prescription, implemented by modification of the g-factors (Brown and Wildenthal, 1987) that is multiplied to the SNMEs to obtain $B(M1)$. Here, we applied the same empirical quenching factor as used in the modification of g-factors to the SNMEs calculated by the shell model. The results are shown by the dotted lines (USDB$^{\text{eff}}$) in **Figure 8**. The empirical quenching factors are similar between IS and IV transitions. SNMEs of the IV spin-$M1$ transitions with the empirical quenching factor turned out to be compatible with the data.

In contrast, description of the IS transitions became worse by introducing the empirical quenching factor. The present result shows that the widely-used effective g-factors lead to an over-quenching of the IS spin component of the $M1$transition in the sd-shell. It should be noted that the observed $B(M1)$ strength of the 1^+ excited state at 10.23 MeV in ^{48}Ca by (p,p') scattering is more consistent with electron scattering data when no quenching is assumed for the IS part of the transition strength (Birkhan et al., 2016; Mathy et al., 2017). A recent theoretical work (Sagawa et al., 2016; Sagawa and Suzuki, 2018) reported that both the IS and IV SNMEs can be reproduced (short dashed line) by enhancing the IS spin-triplet pairing matrices by a factor of 1.1 in addition to applying the empirical quenching factor to the IV spin-$M1$ operator but not the IS spin-$M1$ operator (USDB*qiv). Note that in (Sagawa and Suzuki, 2018) the USDB*qiv result for the IS spin-$M1$ excitations is not shown, but it is the same as USDB*. The theoretical work implies that the present description of the shell model using USD interactions and the empirical quenching factors may have room to be improved in the IS spin-triplet interaction channel and in the IS quenching factor.

5.3 Isoscalar Magnetic Moments

In this section, we discuss how the new finding of quenching of the IS and IV spin-$M1$ SNMEs is understood in relation to the IS and IV magnetic moment studied in the past. The magnetic moment is described by the diagonal component of the nuclear matrix element with the relevant $M1$ operator while the $M1$ transitions correspond to the off-diagonal components as described in **Section 2**.

The experimental $\langle S \rangle$ data are plotted in the left panel of **Figure 9**, and the squared values in the right panel. The $\langle S \rangle$ values calculated by the shell model with the effective IS g-factors (Brown and Wildenthal, 1983; Brown and Wildenthal, 1987) using the USD interaction are indicated by open circles and crosses for the bare and effective g factors, respectively. The results show clear discrepancies between the experimental data and the prediction with the bare g-factor, corresponding to the quenching, in the edge regions of the sd-shell (A = 17–19 and 35–39) close to the magic numbers of A = 16 and 40. The difference is, however, not obvious in the mid-shell region

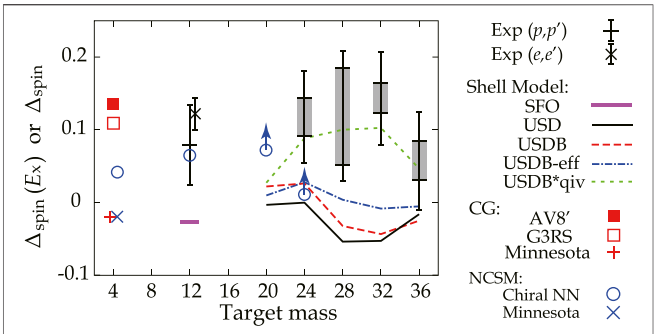

FIGURE 10 | Experimental data of Δ_{spin} (E_x) summed up to E_x = 16 MeV are plotted for proton (electron) scattering by the horizontal bars (cross mark) with the error bars. The definitions of error bars and gray bands are the same as in **Figure 8**. Theoretical predictions of $\Delta_{spin}=\langle \vec{S}_p \cdot \vec{S}_n \rangle$ are plotted for the shell models, Correlated Gaussian (CG) method (Suzuki et al., 2008), and No-Core Shell-Model (NCSM) (Roth et al., 2010). The figure was taken from Matsubara et al. (2015) with updated predictions from Sagawa and Suzuki (2018).

(A = 21–31). The discrepancies in the edge regions are reduced by introduction of the effective IS *g*-factors. The IS magnetic moments in the mid-shell region are reasonably reproduced without introducing the effective IS *g*-factors, which is consistent with our finding of no quenching of the IS spin-*M*1 SNMEs.

5.4 Proton-Neutron Spin-Spin Correlation in the Ground State

Figure 10 shows the Δ_{spin} (E_x) data summed up to E_x=16 MeV by the solid bars. Electron scattering data (von Neumann-Cosel et al., 2000) is plotted at A = 12 by the black cross mark with the error bar, which is consistent with the proton scattering data within experimental uncertainty. It is interesting to note that all the experimental data show positive numbers. The Δ_{spin} values at A = 4 predicted by Correlated Gaussian (CG) method (Suzuki et al., 2008), an ab initio approach, are plotted for each of the *NN* interactions of AV8' (red solid square), G3RS (red open square) and Minnesota (red plus). The predictions by the No-Core Shell-Model (NCSM) (Roth et al., 2010) are plotted for chiral *NN* (Entem and Machleidt, 2003) (blue open circle) and Minnesota (blue cross) interactions. Both predictions using the Minnesota interaction are consistent with each other and are slightly negative. The Minnesota interaction does not contain tensor interactions. It is illuminating to see that the predictions are positive when more realistic *NN* interactions are used: AV8' (Pudliner et al., 1997) and G3RS (Tamagaki, 1968) interactions for the CG method and chiral *NN* interaction (Entem and Machleidt, 2003) for NCSM. The shell model predictions of Δ_{spin} at A = 12 with SFO interaction (solid horizontal line) and A = 20–36 with USD interaction are slightly negative or close to zero, which is significantly smaller than the experimental data of Δ_{spin}. The trend of the USDB interaction (dashed line) is similar. The predicted values increase a little but are still much smaller than the experimental results when the IS and IV effective quenching factors determined in the study of the *g*-factors (Brown and Wildenthal, 1987) are applied to the SNME predicted by the shell model (dot-dashed line). The situation is similar for the other studies of effective *g*-factors (Towner and Khanna, 1983; Arima et al., 1987; Towner, 1987). The experimental data are reproduced when IS spin-triple pairing matrices are enhanced by a factor of 1.1, and only the IV part of SNME is quenched by effective quenching factors (dotted line) (Sagawa and Suzuki, 2018).

NCSM with the chiral *NN* interaction predicts Δ_{spin} values for ^{20}Ne (N_{MAX} = 4) and ^{24}Mg (N_{MAX} = 2), as indicated by the open blue circles in **Figure 10**. Here, N_{MAX} defines the maximal allowed harmonic-oscillator excitation energy above the unperturbed ground state (Roth et al., 2010), hence representing a measure of the model space. Variation of the values depending on N_{MAX} shows a clear trend toward positive when N_{MAX} increases: −0.007, 0.028, and 0.072 for N_{MAX} = 0, 2 and 4 for ^{20}Ne and −0.018 and 0.011 for N_{MAX}=0 and 2 for ^{24}Mg, respectively. Although the values are not converged yet, they are taken as a lower limit in the plot (expressed by arrows). The increase of Δ_{spin} with increasing N_{MAX} implies that mixing of higher-lying orbits is important for reproducing the $\Delta_{spin} > 0$ values.

The observed positive Δ_{spin} value implies that deuteron-like correlated *np* pairs are formed in the ground state of the target nuclei. Note that Δ_{spin} takes a value of 1/4 for the IS *np* pair like a deuteron, −3/4 for the IV *np* pair, and zero for uncorrelated *np* pairs. Thus the IS *np* pairs are favored over the IV *np* pairs. It would be interesting to see how Δ_{spin} values are predicated by ab initio calculations (Gysbers et al., 2019) that reproduce the GT transition strengths studied by beta-decay without a quenching factor by introducing the contribution from the two-body current and many-body correlations. The finding would have relevance to the observed *np* pair dominance in the correlated *NN* pairs with high relative momentum in nuclei observed by electron scattering (Subedi et al., 2008; Hen et al., 2014; Hen et al., 2017) or by ^{16}O(p, d) reactions (Ong et al., 2013; Terashima et al., 2018). The electron scattering data probe all the components of the correlated *NN* pairs due to the high incident energy of the electrons without limitation placed on the excitation energy of the residual nucleus after knockout of a correlated *NN* pair. In contrast, the ^{16}O(p, d) data would be relevant to the *NN* pairs at around the Fermi surface of the target nucleus since the excitation energy of the residual nucleus is limited in the region of several MeV. The present experimental data of Δ_{spin} (E_x) are also limited to 16 MeV and thus are considered to be sensitive to the spin-spin correlation in the *np* pairs at around the Fermi surface. The spin-aligned IS *np* coupling of the valence particles in ^{92}Pd was studied from the level structure determined by gamma spectroscopy (Cederwall et al., 2011), which also indicates the effect of IS *np* pairs at around the Fermi surface. It would be interesting to extend the study of Δ_{spin} (E_x) to higher-excitation energies to observe how the *np* spin-spin correlation changes in deeper single particle orbits.

6 SUMMARY

In summary, spin-$M1$ excitation in nuclei is important for the study of NC neutrino reactions in astrophysical phenomena and in neutrino detectors. Quenching of the IS and IV spin-$M1$ SNMEs for $N = Z$ sd-shell nuclei has been studied by high energy-resolution measurement of proton inelastic scattering up to the excitation energy of 16 MeV. No quenching of the IS spin-$M1$ SNMEs has been observed in the measured nuclei, while the IV spin-$M1$ SNMEs are quenched by an amount comparable with the analogous GT transitions. Consistency with the study of the IS and IV magnetic moment in the same mass region has been discussed. It has been shown by applying the sum rule values that the difference of the IS and IV spin-$M1$ SNMEs is relevant to the np spin-spin correlation in the ground state. Thus, quenching of the IS and IV spin-$M1$ SNMEs needs to be described in a mutually consistent manner by theoretical models. The np spin-spin correlation would have a relevance to the correlated np pair with high relative momentum studied by electron scattering and (p, d) reactions as well as to the spin-aligned IS np coupling. It would be of interest to extend the present study to higher excitation energies and to mass and isotope dependencies. For example, decomposition of the spin-M1 strength in the continuum might be applicable by the multipole decomposition analysis of the angular distribution in combination with an isoscalar probe like deuteron scattering or with a pure isovector probe like (p, n). It is worth considering the measurement of $(^{12}\mathrm{C},^{12}\mathrm{C}^{*})$ reactions for studying each of the IS and IV spin-flip excitations of the target nucleus by tagging the IS and IV 1^{+} states of the ejectile with the coincidence detection of the α or γ emission. Also a measurement in inverse kinematics with an active target based on a time projection chamber would be able to extend the study to larger masses than 40 by employing radioactive secondary beams.

We note that a theoretical work (Isacker and Macchiavelli, 2021) appeared during the review process of this article. That study reported that the positive Δ_{spin} values, referred as $\langle \vec{S}_n \cdot \vec{S}_p \rangle$ in their paper, were not reproduced by Hamiltonian for all the possible parameter values describing neutrons and protons interacting in a single-l shell through a surface delta interaction. Theoretical interpretation of the positive values is still an open question.

DATA AVAILABILITY STATEMENT

The raw data supporting the conclusions of this article will be made available by the authors, without undue reservation.

AUTHOR CONTRIBUTIONS

All authors listed have made a substantial, direct, and intellectual contribution to the work and approved it for publication.

FUNDING

This work was supported by the JSPS International Training Program (ITP) and was partially supported by JSPS (No. 14740154, and 25105509).

ACKNOWLEDGMENTS

The authors gratefully acknowledge the collaborators of the E249 and E299 experiments at the RCNP. They are indebted to the RCNP cyclotron staff for providing us with the excellent beam. We are grateful to Sagawa, Nakada, and Ichimura for valuable discussions.

REFERENCES

Alburger, D. E., and Nathan, A. M. (1978). Beta-Ray Branching and Half-Lives of ^{12}B and ^{12}N. *Phys. Rev. C* 17, 280–286. doi:10.1103/PhysRevC.17.280

Anantaraman, N., Brown, B. A., Crawley, G. M., Galonsky, A., Djalali, C., Marty, N., et al. (1984). Observation of Quenching in Isoscalar and Isovector 0+ → 1+ Transitions in Si28(p,p′). *Phys. Rev. Lett.* 52, 1409–1412. doi:10.1103/PhysRevLett.52.1409

Anderson, B. D., Chittrakarn, T., Baldwin, A. R., Lebo, C., Madey, R., Tandy, P. C., et al. (1987). Gamow-Teller and M1 Strength in the 32S(p,n)32Cl Reaction at 135 Mev. *Phys. Rev. C. Nucl. Phys.* 36, 2195–2205. doi:10.1103/physrevc.36.2195

Arima, A., Shimizu, K., Bentz, W., and Hyuga, H. (1987). Nuclear Magnetic Properties and Gamow-Teller Transitions. *Adv. Nucl. Phys.* 18, 1–106.

Bendel, W. L., Fagg, L. W., Numrich, S. K., Jones, E. C., and Kaiser, H. F. (1971). Excitation of by 180 Electron Scattering. *Phys. Rev. C* 3, 1821–1827. doi:10.1103/PhysRevC.3.1821

Bernabéu, J., Ericson, T., Hernández, E., and Ros, J. (1992). Effects of the Axial Isoscalar Neutral-Current for Solar Neutrino Detection. *Nucl. Phys. B* 378, 131–149. doi:10.1016/0550-3213(92)90006-W

Birkhan, J., Matsubara, H., von Neumann-Cosel, P., Pietralla, N., Ponomarev, V. Y., Richter, A., et al. (2016). Electromagnetic M 1 Transition Strengths from Inelastic Proton Scattering: The Cases of ca 48 and pb 208. *Phys. Rev. C* 93, 041302. doi:10.1103/PhysRevC.93.041302

Brown, B., and Rae, W. (2014). The Shell-Model Code Nushellx@msu. *Nucl. Data Sheets* 120, 115–118. doi:10.1016/j.nds.2014.07.022

Brown, B., and Wildenthal, B. (1987). Empirically Optimum m1 Operator for sd-Shell Nuclei. *Nucl. Phys. A* 474, 290–306. doi:10.1016/0375-9474(87)90619-1

Brown, B. A., and Richter, W. A. (2006). New "usd" Hamiltonians for the *sd* Shell. *Phys. Rev. C* 74, 034315. doi:10.1103/PhysRevC.74.034315

Brown, B. A., and Wildenthal, B. H. (1983). Corrections to the Free-Nucleon Values of the Single-Particle Matrix Elements of the $m1$ and Gamow-Teller Operators, From a Comparison of Shell-Model Predictions With -Shell Data. *Phys. Rev. C* 28, 2397–2413. doi:10.1103/PhysRevC.28.2397

Cederwall, B., Moradi, F. G., Bäck, T., Johnson, A., Blomqvist, J., Clément, E., et al. (2011). Evidence for a Spin-Aligned Neutron–Proton Paired Phase From the Level Structure of 92 pd. *Nature* 469, 68–71. doi:10.1038/nature09644

Cohen, S., and Kurath, D. (1965). Effective Interactions for the 1p Shell. *Nucl. Phys.* 73, 1–24. doi:10.1016/0029-5582(65)90148-3

Cooper, E. D., Hama, S., and Clark, B. C. (2009). Global Dirac Optical Potential from Helium to lead. *Phys. Rev. C* 80, 034605. doi:10.1103/PhysRevC.80.034605

Crawley, G. M., Djalali, C., Marty, N., Morlet, M., Willis, A., Anantaraman, N., et al. (1989). Isovector and Isoscalar Spin-Flip Excitations in Even-Even s-d Shell Nuclei Excited by Inelastic Proton Scattering. *Phys. Rev. C* 39, 311–323. doi:10.1103/PhysRevC.39.311

Edmonds, A. (1960). *Angular Momentum in Quantum Mechanics*. Princeton, NJ: Princeton University Press.

Entem, D. R., and Machleidt, R. (2003). Accurate Charge-Dependent Nucleon-Nucleon Potential at Fourth Order of Chiral Perturbation Theory. *Phys. Rev. C* 68, 041001. doi:10.1103/PhysRevC.68.041001

Firestone, R. (1996). *Table of Isotopes*. 8th Edn. New York: John Wiley & Sons.

Foltz, C. W., Sober, D. I., Fagg, L. W., Gräf, H. D., Richter, A., Spamer, E., et al. (1994). Electroexcitation of Low-Multipolarity Magnetic Transitions in ^{36}Ar and ^{38}Ar. *Phys. Rev. C* 49, 1359–1371. doi:10.1103/PhysRevC.49.1359

Franey, M. A., and Love, W. G. (1985). Nucleon-Nucleon t-Matrix Interaction for Scattering at Intermediate Energies. *Phys. Rev. C* 31, 488–498. doi:10.1103/PhysRevC.31.488

Fujita, H., Fujita, Y., Adachi, T., Bacher, A. D., Berg, G. P. A., Black, T., et al. (2007). Isospin Structure of States in ^{58}Ni and ^{58}Cu Studied by ^{58}Ni(p, p') and ^{58}Ni(^{3}He,t)^{58}Cu Measurements. *Phys. Rev. C* 75, 034310. doi:10.1103/PhysRevC.75.034310

Fujita, H., Fujita, Y., Berg, G., Bacher, A., Foster, C., Hara, K., et al. (2002). Realization of Matching Conditions for High-Resolution Spectrometers. *Nucl. Instr. Methods Phys. Res. A: Acc. Spectr. Detect. Assoc. Equip.* 484, 17–26. doi:10.1016/S0168-9002(01)01970-2

Fujita, Y., Brown, B. A., Ejiri, H., Katori, K., Mizutori, S., and Ueno, H. (2000). Separation of Isoscalar, Isovector, Orbital, and Spin Contributions in Transitions in Mirror Nuclei. *Phys. Rev. C* 62, 044314. doi:10.1103/PhysRevC.62.044314

Fujita, Y., Fujita, H., Adachi, T., Berg, G. P. A., Caurier, E., Fujimura, H., et al. (2002). Gamow-Teller Transitions From ^{58}Ni to Discrete States of ^{58}Cu - The Study of Isospin Symmetry in Atomic Nuclei. *Eur. Phys. J. A.* 13, 411–418. doi:10.1140/epja/iepja1344

Fujita, Y., Hatanaka, K., Berg, G., Hosono, K., Matsuoka, N., Morinobu, S., et al. (1997). Matching of a Beam Line and a Spectrometer New Beam Line Project at rcnp. *Nucl. Instr. Methods Phys. Res. B: Beam Inter. Mater. Atoms* 126, 274–278. doi:10.1016/S0168-583X(96)01008-7

Fujita, Y., Rubio, B., and Gelletly, W. (2011). Spin-Isospin Excitations Probed by Strong, Weak and Electro-Magnetic Interactions. *Prog. Part. Nucl. Phys.* 66, 549–606. doi:10.1016/j.ppnp.2011.01.056

Fujiwara, M., Akimune, H., Daito, I., Fujimura, H., Fujita, Y., Hatanaka, K., et al. (1999). Magnetic Spectrometer Grand Raiden. *Nucl. Instr. Methods Phys. Res. A* 422, 484–488. doi:10.1016/S0168-9002(98)01009-2

Gysbers, P., Hagen, G., Holt, J., Jansen, G. R., Morris, T. D., Navrátil, P., et al. (2019). Discrepancy Between Experimental and Theoretical β-Decay Rates Resolved From First Principles. *Nat. Phys.* 15, 428–431. doi:10.1038/s41567-019-0450-7

Hen, O., Miller, G. A., Piasetzky, E., and Weinstein, L. B. (2017). Nucleon-Nucleon Correlations, Short-Lived Excitations, and the Quarks Within. *Rev. Mod. Phys.* 89, 045002. doi:10.1103/RevModPhys.89.045002

Hen, O., Sargsian, M., Weinstein, L. B., Piasetzky, E., Hakobyan, H., Higinbotham, D. W., et al. (2014). Momentum Sharing in Imbalanced Fermi Systems. *Science* 346, 614–617. doi:10.1126/science.1256785

Hofmann, F., von Neumann-Cosel, P., Neumeyer, F., Rangacharyulu, C., Reitz, B., Richter, A., et al. (2002). Magnetic Dipole Transitions in ^{32}S From Electron Scattering at 180. *Phys. Rev. C* 65, 024311. doi:10.1103/PhysRevC.65.024311

Ichimura, M., Sakai, H., and Wakasa, T. (2006). Spin-Isospin Responses via (p,n) and (n,p) Reactions. *Prog. Part. Nucl. Phys.* 56, 446–531. doi:10.1016/j.ppnp.2005.09.001

Ikeda, K., Fujii, S., and Fujita, J. (1963). The (p,n) Reactions and Beta Decays. *Phys. Lett.* 3, 271–272. doi:10.1016/0031-9163(63)90255-5

Isacker, P. V., and Macchiavelli, A. (2021). Neutron-proton Spin-Spin Correlations in the Ground States of Nuclei. *Eur. Phys. J.* 57, 178. doi:10.1140/epja/s10050-021-00489-6

Kawabata, T., Akimune, H., Fujimura, H., Fujita, H., Fujita, Y., Fujiwara, M., et al. (2004). Isovector and Isoscalar Spin-Flip Strengths in ^{11}B. *Phys. Rev. C* 70, 034318. doi:10.1103/PhysRevC.70.034318

Kirson, M. W. (2007). Oscillator Parameters in Nuclei. *Nucl. Phys. A* 781, 350–362. doi:10.1016/j.nuclphysa.2006.10.077

Love, W. G., and Franey, M. A. (1981). Effective Nucleon-Nucleon Interaction for Scattering at Intermediate Energies. *Phys. Rev. C* 24, 1073–1094. doi:10.1103/PhysRevC.24.1073

Lüttge, C., Neumann-Cosel, Pv., Neumeyer, F., Rangacharyulu, C., Richter, A., Schrieder, G., et al. (1996). Isovector m1 Transitions in and the Role of Meson Exchange Currents. *Phys. Rev. C* 53, 127–130. doi:10.1103/PhysRevC.53.127

Mathy, M., Birkhan, J., Matsubara, H., von Neumann-Cosel, P., Pietralla, N., Ponomarev, V. Y., et al. (2017). Search for Weak m 1 Transitions in ca 48 With Inelastic Proton Scattering. *Phys. Rev. C* 95, 054316. doi:10.1103/PhysRevC.95.054316

Matsubara, H. (2010). Isoscalar and isovector spin-M1 transitions from the even-even, N = Z nuclei across the sd-shell region. PhD thesis. Toyonaka: Osaka University.

Matsubara, H., Sakaguchi, H., Kishi, T., and Tamii, A. (2009). Self-supporting Elemental Sulfur Target for Charged Particle Irradiation. *Nucl. Instr. Methods Phys. Res. B* 267, 3682–3687. doi:10.1016/j.nimb.2009.09.002

Matsubara, H., Tamii, A., Nakada, H., Adachi, T., Carter, J., Dozono, M., et al. (2015). Nonquenched Isoscalar Spin- Excitations in -Shell Nuclei. *Phys. Rev. Lett.* 115, 102501. doi:10.1103/PhysRevLett.115.102501

Matsubara, H., Tamii, A., Shimizu, Y., Suda, K., Tameshige, Y., and Zenihiro, J. (2012). Wide-Window Gas Target System for High Resolution experiment with Magnetic Spectrometer. *Nucl. Instr. Methods Phys. Res. A* 678, 122–129. doi:10.1016/j.nima.2012.03.005

Ong, H., Tanihata, I., Tamii, A., Myo, T., Ogata, K., Fukuda, M., et al. (2013). Probing Effect of Tensor Interactions in 16o via (p,d) Reaction. *Phys. Lett. B* 725, 277–281. doi:10.1016/j.physletb.2013.07.038

Petrovich, F., and Love, W. (1981). The Scattering of Elementary Probes From Nuclei at Medium Energy: A New Look at the Nucleus. *Nucl. Phys. A* 354, 499–534. doi:10.1016/0375-9474(81)90613-8

Pudliner, B. S., Pandharipande, V. R., Carlson, J., Pieper, S. C., and Wiringa, R. B. (1997). Quantum Monte Carlo Calculations of Nuclei With A <= 7. *Phys. Rev. C* 56, 1720–1750. doi:10.1103/PhysRevC.56.1720

Raynal, J. (2007). Computer Code dwba07. Report No. NEA-1209/008.

Richter, A., Weiss, A., Haüsser, O., and Brown, B. A. (1990). New Evidence for Meson-Exchange-Current Enhancement of Isovector M1 Strength. *Phys. Rev. Lett.* 65, 2519–2522. doi:10.1103/PhysRevLett.65.2519

Richter, W. A., Mkhize, S., and Brown, B. A. (2008). *sd*-Shell Observables for the usda and usdb Hamiltonians. *Phys. Rev. C* 78–064302. doi:10.1103/PhysRevC.78.064302

Roth, R., Neff, T., and Feldmeier, H. (2010). Nuclear Structure in the Framework of the Unitary Correlation Operator Method. *Prog. Part. Nucl. Phys.* 65, 50–93. doi:10.1016/j.ppnp.2010.02.003

Sagawa, H., and Suzuki, T. (2018). Isoscalar and Isovector Spin Response in -Shell Nuclei. *Phys. Rev. C* 97, 054333. doi:10.1103/PhysRevC.97.054333

Sagawa, H., Suzuki, T., and Sasano, M. (2016). Effect of Isoscalar Spin-Triplet Pairings on Spin-Isospin Responses in s d-Shell Nuclei. *Phys. Rev. C* 94, 041303. doi:10.1103/PhysRevC.94.041303

Sasano, M., Sakai, H., Yako, K., Wakasa, T., Asaji, S., Fujita, K., et al. (2009). Gamow-teller Unit Cross Sections of the Reaction at 198 and 297 mev on Medium-Heavy Nuclei. *Phys. Rev. C* 79, 024602. doi:10.1103/PhysRevC.79.024602

Subedi, R., Shneor, R., Monaghan, P., Anderson, B., Aniol, K., Annand, J., et al. (2008). Probing Cold Dense Nuclear Matter. *Science* 320, 1476–1478. doi:10.1126/science.1156675

Suzuki, T., Fujimoto, R., and Otsuka, T. (2003). Gamow-Teller Transitions and Magnetic Properties of Nuclei and Shell Evolution. *Phys. Rev. C* 67, 044302. doi:10.1103/PhysRevC.67.044302

Suzuki, Y., Horiuchi, W., Orabi, M., and Arai, K. (2008). Global-vector Representation of the Angular Motion of Few-Particle Systems ii. *Few-Body Syst.* 42. doi:10.1007/s00601-008-0200-3

Taddeucci, T., Goulding, C., Carey, T., Byrd, R., Goodman, C., Gaarde, C., et al. (1987). The (p,n) Reaction as a Probe of Beta Decay Strength. *Nucl. Phys. A* 469, 125–172. doi:10.1016/0375-9474(87)90089-3

Taddeucci, T. N., Byrd, R. C., Carey, T. A., Ciskowski, D. E., Foster, C. C., Gaarde, C., et al. (1990). Gamow-teller Transition Strengths from the ^{11}B(p,nc) Reaction in the Energy Range 160–795 mev. *Phys. Rev. C* 42, 935–946. doi:10.1103/PhysRevC.42.935

Tamagaki, R. (1968). Potential Models of Nuclear Forces at Small Distances. *Prog. Theor. Phys.* 39, 91–107. doi:10.1143/PTP.39.91

Tamii, A., Akimune, H., Daito, I., Fujita, Y., Fujiwara, M., Hatanaka, K., et al. (1999). Polarization Transfer Observables for Proton Inelastic Scattering from 12c at 0. *Phys. Lett. B* 459, 61–66. doi:10.1016/S0370-2693(99)00654-1

Tamii, A., Fujita, Y., Matsubara, H., Adachi, T., Carter, J., Dozono, M., et al. (2009). Measurement of High Energy Resolution Inelastic Proton Scattering at and Close to Zero Degrees. *Nucl. Instrum.Methods Phys. Res. Sect. A.* 605, 326–338. doi:10.1016/j.nima.2009.03.248

Terashima, S., Yu, L., Ong, H. J., Tanihata, I., Adachi, S., Aoi, N., et al. (2018). Dominance of Tensor Correlations in High-Momentum Nucleon Pairs Studied by Reaction. *Phys. Rev. Lett.* 121, 242501. doi:10.1103/PhysRevLett.121.242501

Towner, I., and Khanna, F. (1983). Corrections to the Single-Particle m1 and Gamow-Teller Matrix Elements. *Nucl. Phys. A* 399, 334–364. doi:10.1016/0375-9474(83)90252-X

Towner, I. (1987). Quenching of Spin Matrix Elements in Nuclei. *Phys. Rep.* 155, 263–377. doi:10.1016/0370-1573(87)90138-4

von Neumann-Cosel, P., and Tamii, A. (2019). Electric and Magnetic Dipole Modes in High-Resolution Inelastic Proton Scattering at 0. *Eur. Phys. J. A* 55. doi:10.1140/epja/i2019-12781-7

von Neumann-Cosel, P., Gräf, H. D., Krämer, U., Richter, A., and Spamer, E. (2000). Electroexcitation of Isoscalar and Isovector Magnetic Dipole Transitions in 12c and Isospin Mixing. *Nucl. Phys. A* 669 3–13. doi:10.1016/S0375-9474(99)00564-3

Wakasa, T., Hatanaka, K., Fujita, Y., Berg, G., Fujimura, H., Fujita, H., et al. (2002). High Resolution Beam Line for the Grand Raiden Spectrometer. *Nucl. Instr. Methods Phys. Res. A* 482, 79–93. doi:10.1016/S0168-9002(01)01686-2

Warburton, E. K., and Millener, D. J. (1989). Structure of ^{17}C and ^{17}N. *Phys. Rev. C* 39, 1120–1129. doi:10.1103/PhysRevC.39.1120

Zegers, R. G. T., Akimune, H., Austin, S. M., Bazin, D., van der Berg, A. M., Berg, G. P. A., et al. (2006). The (t,^{3}He) and (^{3}He,t) Reactions as Probes of Gamow-Teller Strength. *Phys. Rev. C* 74, 024309. doi:10.1103/PhysRevC.74.024309

Conflict of Interest: The authors declare that the research was conducted in the absence of any commercial or financial relationships that could be construed as a potential conflict of interest.

The handling editor declared a past co-authorship with one of the authors AT.